Supporting Information

Synergistic Effects of $TiNb_2O_7$-reduced Graphene Oxide Nanocomposite Electrocatalyst for High-performance All-vanadium Redox Flow Battery

Anteneh Wodaje Bayeh,[1] Daniel Manaye Kabtamu,[1] Yu-Chung Chang,[1] Guan-Cheng Chen,[1] Hsueh-Yu Chen,[1] Guan-Yi Lin,[1] Ting-Ruei Liu,[1] Tadele Hunde Wondimu,[1] Kai-Chin Wang,[1] and Chen-Hao Wang*[1,2]

[1] National Taiwan University of Science and Technology, Department of Materials Science and Engineering, Taipei 10607, Taiwan.

[2] Hierarchical Green-Energy Materials (Hi-GEM) Research Center, National Cheng Kung University, Tainan 70101, Taiwan

**Corresponding author, E-mail: chwang@mail.ntust.edu.tw*

Tel: +886-2-2730-3715; Fax: +886-2-2737-6544

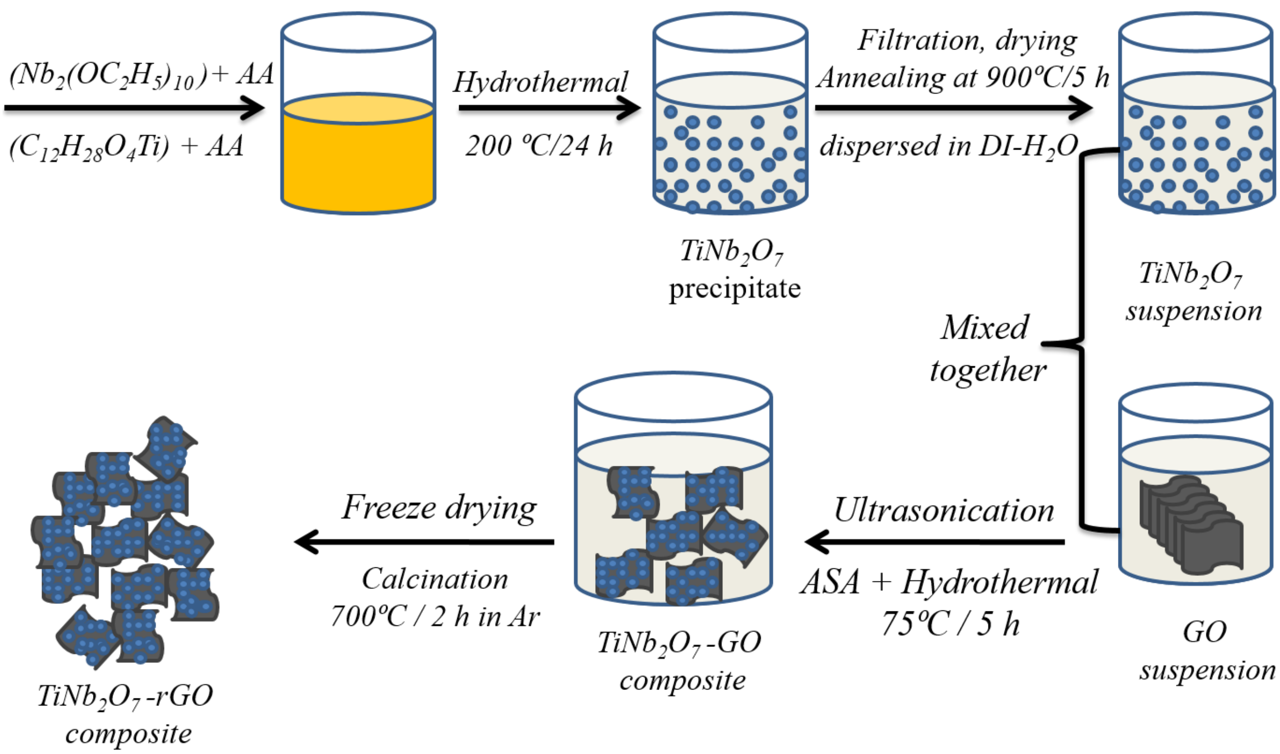

Figure S1 Schematic representation for the synthesis of $TiNb_2O_7$ and $TiNb_2O_7$-rGO nanocomposite materials.

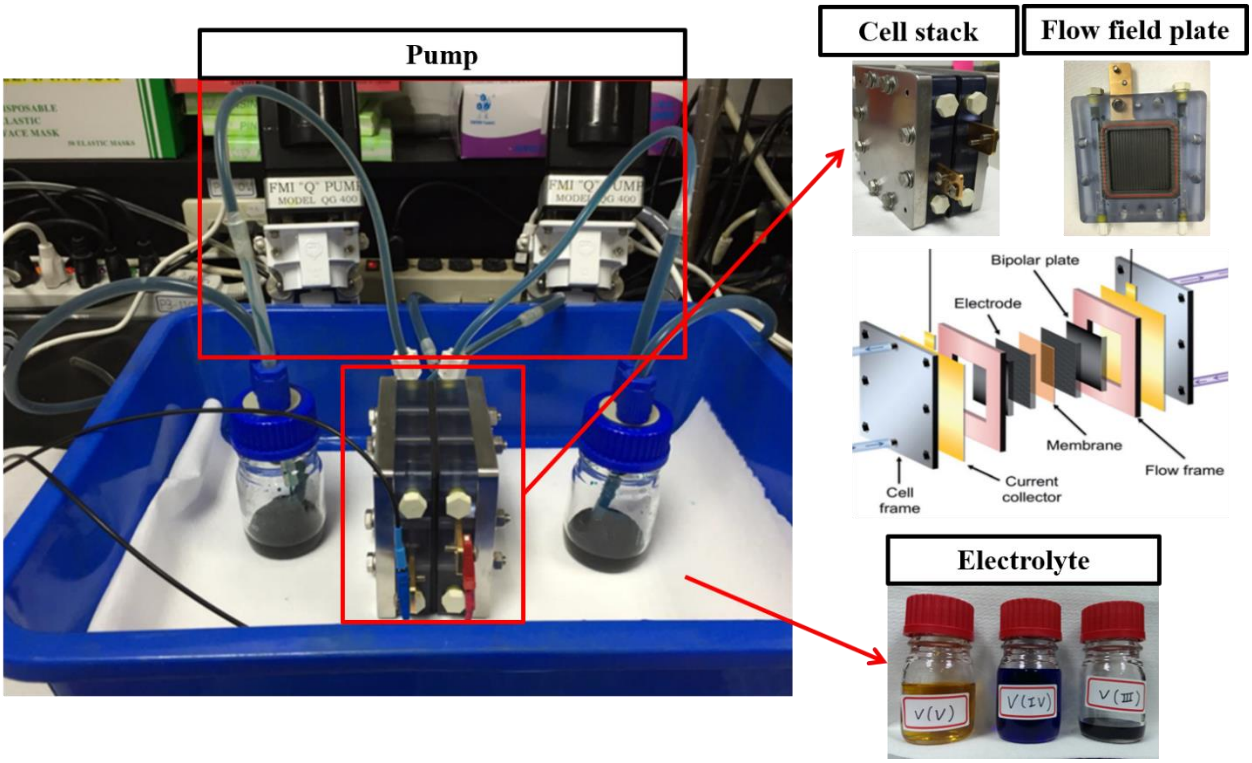

Figure S2 The configurations of single cell test for all VRFBs.

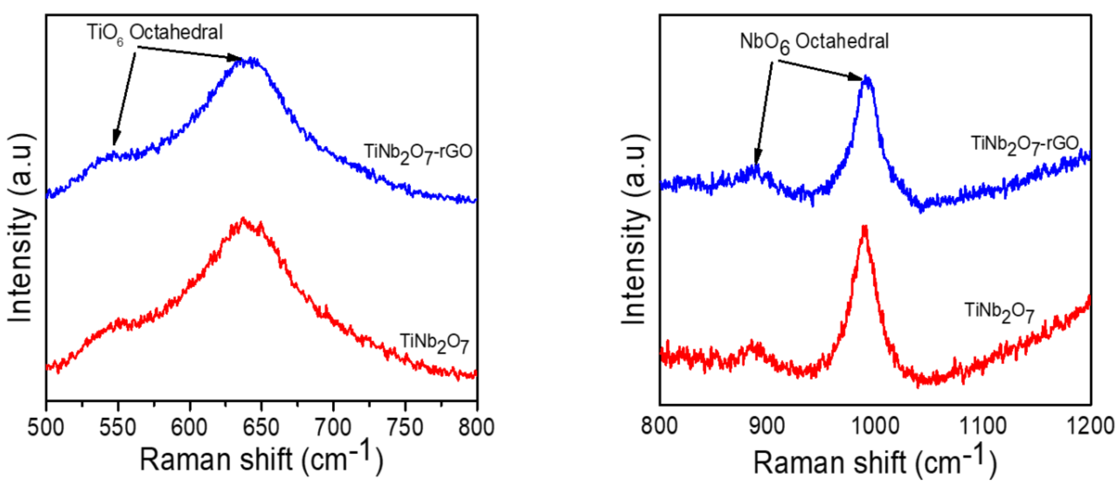

Figure S3 Raman spectra of $TiNb_2O_7$ and $TiNb_2O_7$-rGO (as inset from **Figure 1b**).

The Surface morphologies of GF, and ($TiNb_2O_7$–rGO–GF) were characterized by FESEM. As shown in **Figure S4 a, b** with different magnifications, due to the heat treatment, the GF shows a smooth and clean surface without observable impurities, which can provide suitable substrate for the $TiNb_2O_7$–rGO.[1] **Figure S4 c, d** with lower magnifications show the $TiNb_2O_7$–rGO uniformly covers the surface of the GF. From **Figure S4 e**, **f** at higher magnifications, it is observed that the nanocomposite catalyst is distributed across the rGO surface and cross section of the electrode. The morphology of $TiNb_2O_7$–rGO was in accordance with the Brunauer-Emmett-Teller (BET) results in which a large surface area was recorded for the $TiNb_2O_7$–rGO modified GF electrode.

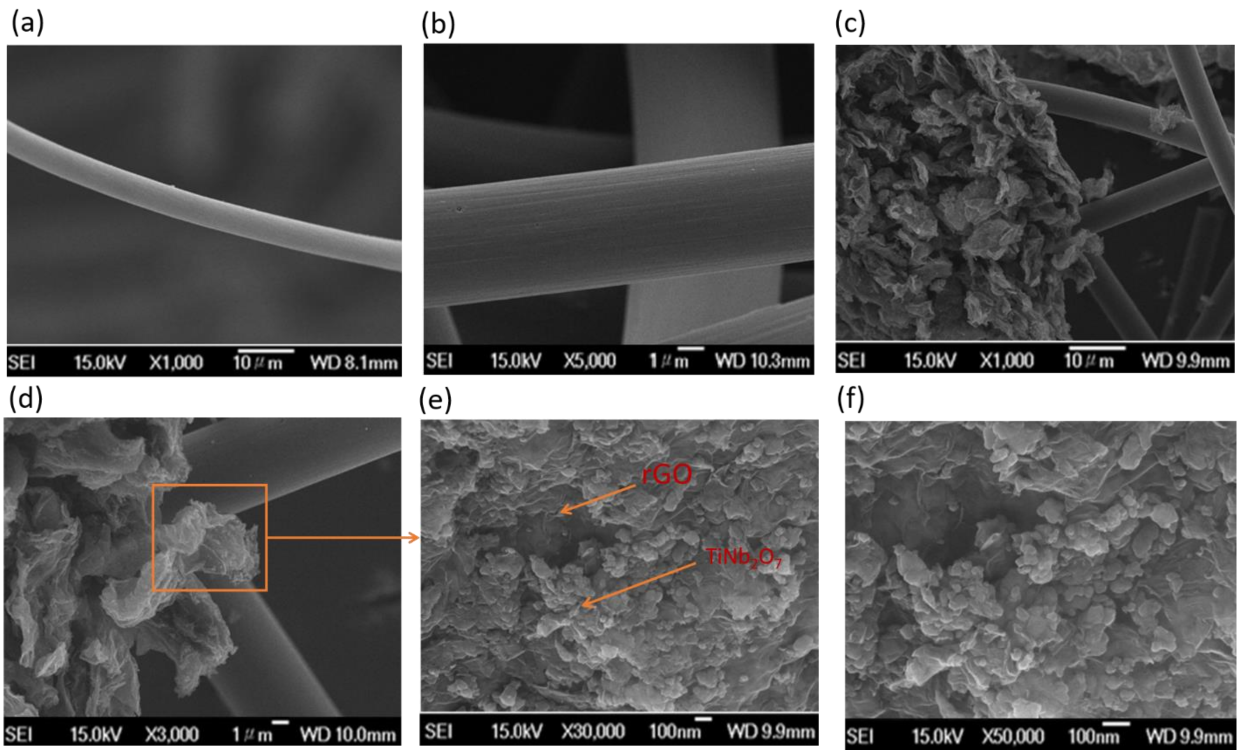

Figure S4: SEM images with different magnifications of (a, b) heat treated pristine GF and (c-f) GF modified with $TiNb_2O_7$–rGO electrocatalyst.

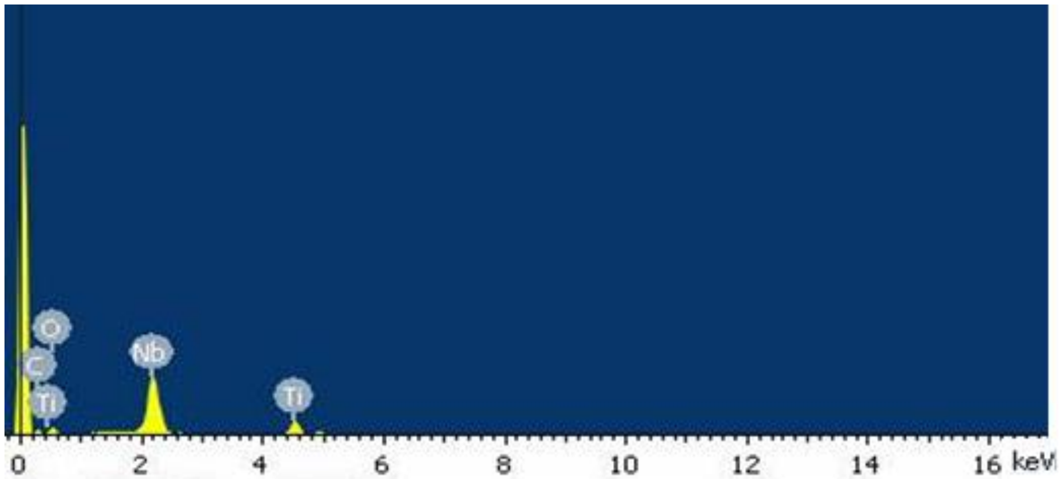

Figure S5 EDX images of $TiNb_2O_7$-rGO.

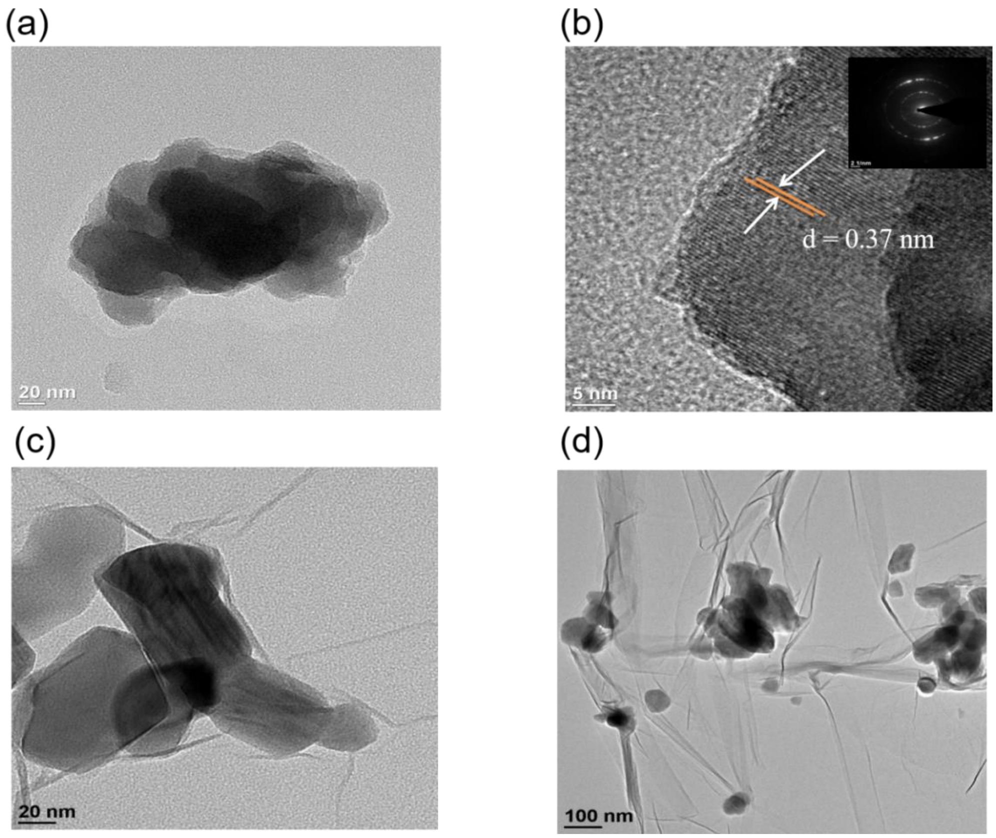

Figure S6 TEM images of (a) pure $TiNb_2O_7$, (c, d) $TiNb_2O_7$-rGO, and (b) HRTEM image of $TiNb_2O_7$.

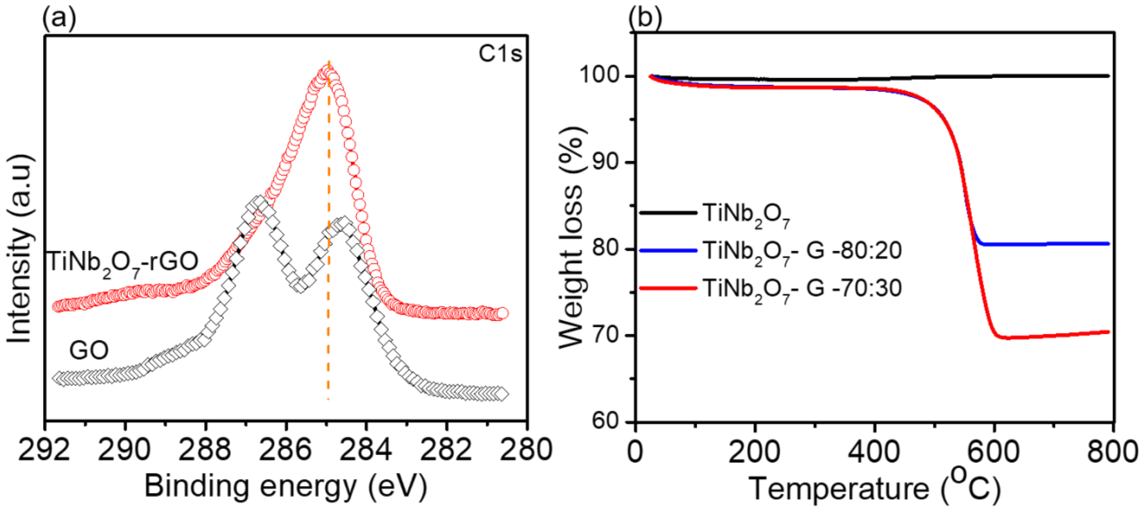

Figure S7 (a) XPS narrow scan C1s in GO and $TiNb_2O_7$-rGO and (b) TGA curves of pure $TiNb_2O_7$ and $TiNb_2O_7$-rGO with different weight ratio.

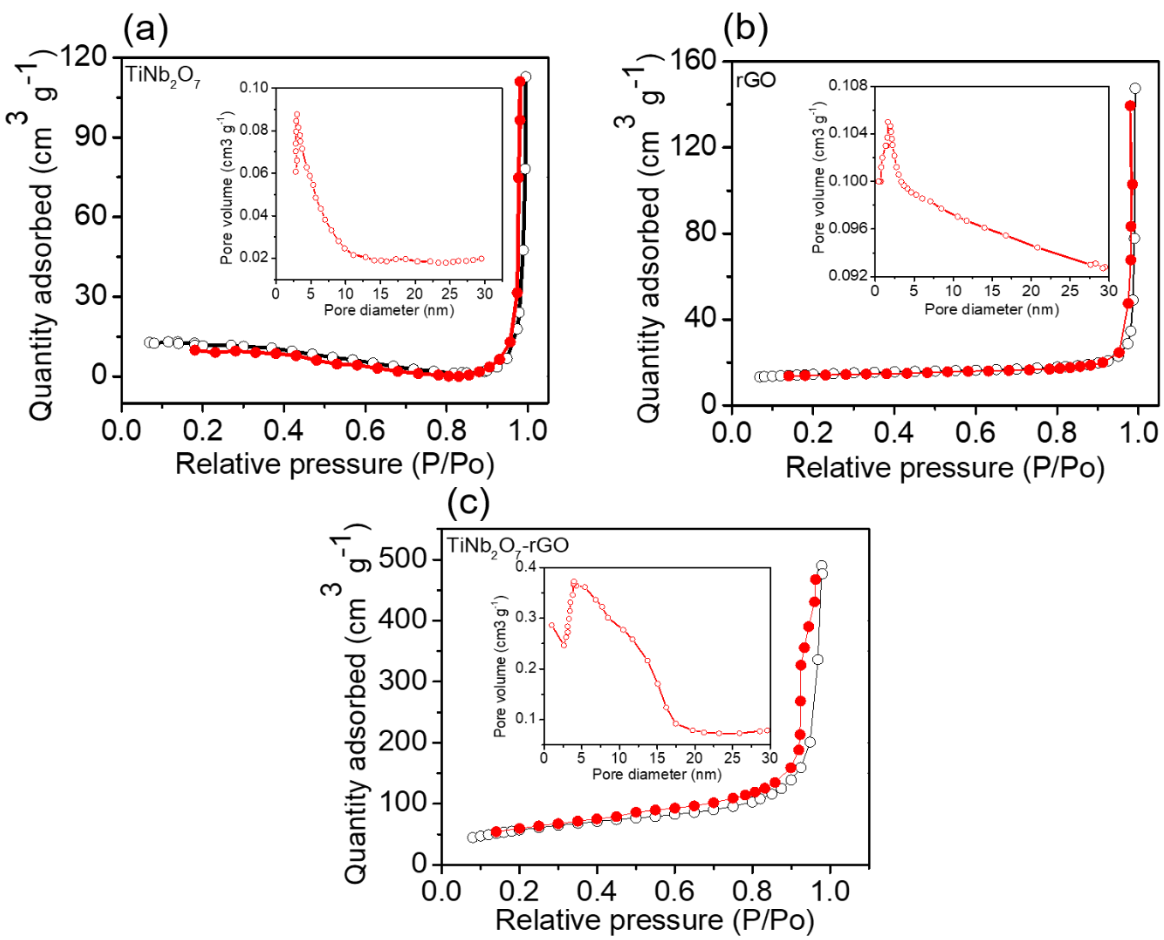

Figure S8 Nitrogen adsorption and desorption isotherms and the corresponding pore size distribution curves of (a) $TiNb_2O_7$, (b) rGO, and (c) $TiNb_2O_7$-rGO.

Table S1 Parameters for all electrocatalyst obtained from **Figure S8**

Sample	S_{BET} (m^2 g^{-1})	Pore volume (cm^3 g^{-1})	Pore size (nm)
$TiNb_2O_7$	16.4	0.0424	12.25
rGO	45.1	0.0994	10.33
$TiNb_2O_7$–rGO	204	0.242	7.80

Table S2 Electrochemical properties result obtained from CV curves (**Figure 5a**).

Electrode	J_{pa}(mA cm^{-2})	J_{pc} (mA cm^{-2})	E_{pa} (V)	E_{pc} (V)	ΔE_p (mV)
$TiNb_2O_7$	---	----	----	----	----
rGO	13.7	-47.5	0.523	0.208	315
$TiNb_2O_7$-rGO	24	-48	0.453	0.208	245

Table S3 Electrochemical properties result obtained from CV curves (**Figure 5b**).

Electrode	J_{pc} (mA cm^{-2})	J_{pa} (mA cm^{-2})	E_{pc} (V)	E_{pa} (V)	ΔE_p (mV)
$TiNb_2O_7$	-7.5	14.7	1.31	0.963	328
rGO	-8.6	16.1	1.19	1.04	152
$TiNb_2O_7$-rGO	-10.7	20.8	1.19	1.04	150

Table S4 EIS fitting results from **Figure 6a**

Electrode	***R_s (Ω)***	***CPE_1***		***R_{ct} (Ω)***	***CPE_2***	
		CPE_1-T	***CPE_1-P***		***CPE_2-T***	***CPE_2-P***
$TiNb_2O_7$	3.50	6.5E-5	0.826	34.4	0.00842	0.609
rGO	3.37	4.27E-4	0.8474	18.01	0.0332	0.504
$TiNb_2O_7$-rGO	3.75	0.000107	0.8073	13.21	0.11403	0.635

Table S5 EIS fitting results from **Figure 6b**

Electrode	***R_s (Ω)***	***CPE_1***		***R_{ct} (Ω)***	***CPE_2***	
		CPE_1-T	***CPE_1-P***		***CPE_2-T***	***CPE_2-P***
$TiNb_2O_7$	3.96	5.07E-5	0.828	24.6	0.0237	0.543
rGO	3.6	9.4E-5	0.855	16.1	0.0331	0.388
$TiNb_2O_7$-rGO	3.41	0.000134	0.7897	10.72	0.0664	0.4028

Figure S9 shows the fitting results for $TiNb_2O_7$, rGO, and $TiNb_2O_7$–rGO. From the figure we can see that the raw data and the fitting results are perfectly overlap each other which confirms all the parameters after the fitting data are obtained with the lowest possible minimum error.

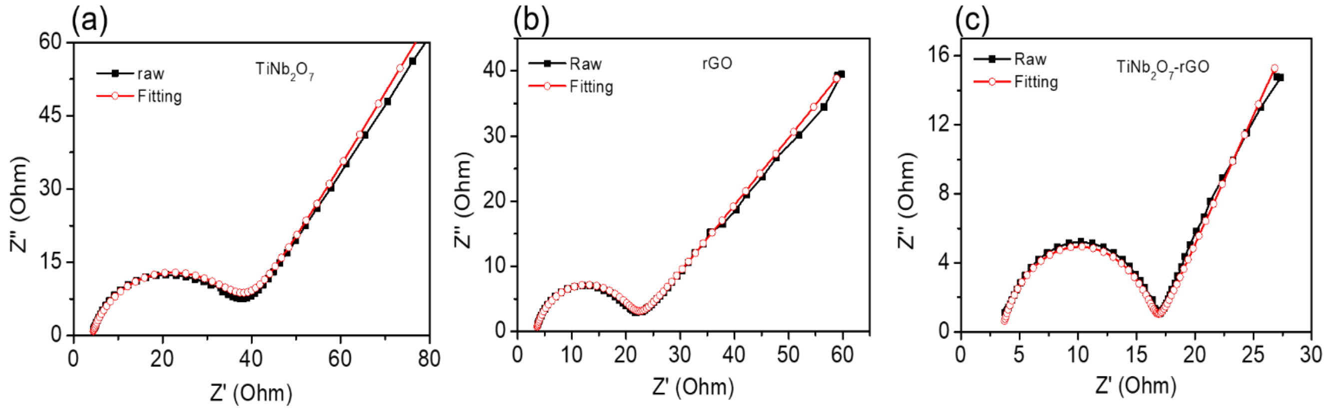

Figure S9 The EIS raw data (black) and fitting results (red) for (a) $TiNb_2O_7$, (b) rGO, and (c) $TiNb_2O_7$–rGO under the polarization potential of 0.5 V.

Table S6 Efficiencies of the cells measured at different current densities.

Electrode	**Current density**	**Average efficiency (%) for cycles**		
	(mA cm^{-2})	**CE**	**VE**	**EE**
	40	93.4	80.1	74.46
	60	93.6	78.2	73.16
	80	94.1	76.54	72.0
GF	100	94.94	73.36	69.64
	120	96.28	70.0	67.36
	140	97.04	66.2	62.28
	160	------	------	-------
	40	93.1	81.3	75.84
	40	93.28	82.4	76.9
$TiNb_2O_7$-GF	60	93.48	80.56	75.3
	80	94.08	78.9	74.2

	100	94.9	75.9	72.0
	120	96.28	72.1	69.5
	140	96.48	69.5	67.1
	160	97	69.9	60.58
	40	93.28	83.86	78.24
	40	93.18	87.2	81.2
	60	93.28	84.6	78.9
	80	94.64	82.7	77.74
	100	95.16	79.0	75.2
rGO-GF	120	96.4	75.7	73.0
	140	97.06	72.5	70.36
	160	97.54	69.6	67.9
	40	93.18	85.8	81.5
	40	93.2	91.6	85.48
	60	93.3	91.3	85.2
	80	94.5	88.1	83.1
$TiNb_2O_7$-rGO-GF	100	95.64	86.2	82.42
	120	96.3	82.7	79.7
	140	96.42	79.5	76.7
	160	97.54	74.1	72.7
	40	93.2	91.9	85.8

Table S7 Comparison of CE, VE and EE of the $TiNb_2O_7$-rGO-GF vs. previously reported materials.

Materials	Electrolyte	Current density *(mA cm^{-2})*	CE *(%)*	VE *(%)*	EE *(%)*	Ref.
WO_3/GF	1 M $VOSO_4$ + 3 M H_2SO_4	100	99.7	72.2	72	[2]
WO_3/SAC	1.5 M $VOSO_4$ + 3 M H_2SO_4	60	95.1	81.5	78.1	[3]
CeO_2/GF	2 M $VOSO_4$ + 2 M H_2SO_4	100	87.9	84.2	74.0	[4]
CeO_2/ECNF	0.85 M $VOSO_4$ + 3 M H_2SO_4	100	-	-	74.5	[5]
MoO_2/MSU-FC	1 M $VOSO_4$ + 1 M H_2SO_4	40	87.6	89.0	87.0	[6]
Mn_3O_4/CF	2 M $VOSO_4$ + 2.5 M H_2SO_4	40	83.5	91.0	76.0	[7]
PbO_2/GF	0.5 M $VOSO_4$ + 3 M H_2SO_4	80	99.7	78.3	78.1	[8]
Ir/CF	0.5 M $VOSO_4$ + 2 M H_2SO_4	20	79.7	87.5	69.7	[9]
Pt/MWNTs	1 M $VOSO_4$ + 1 M H_2SO_4	20	83.9	27.6	23.1	[10]
$TiNb_2O_7$-rGO-GF	1.6 M $VOSO_4$ + 2.5 MH_2SO_4	80	94.5	88.1	83.1	Our
		120	96.3	82.7	79.7	work

References

1. D. M. Kabtamu, J.-Y. Chen, Y.-C. Chang and C.-H. Wang, *Journal of Materials Chemistry A*, 2016, **4**, 11472-11480.
2. Y. Shen, H. Xu, P. Xu, X. Wu, Y. Dong and L. Lu, *Electrochimica Acta*, 2014, **132**, 37-41.
3. C. Yao, H. Zhang, T. Liu, X. Li and Z. Liu, *Journal of Power Sources*, 2012, **218**, 455-461.
4. H. Zhou, J. Xi, Z. Li, Z. Zhang, L. Yu, L. Liu, X. Qiu and L. Chen, *RSC Advances*, 2014, **4**, 61912-61918.
5. M. Jing, X. Zhang, X. Fan, L. Zhao, J. Liu and C. Yan, *Electrochimica Acta*, 2016, **215**, 57-65.
6. H. T. Thu Pham, C. Jo, J. Lee and Y. Kwon, *RSC Advances*, 2016, **6**, 17574-17582.
7. K. J. Kim, M.-S. Park, J.-H. Kim, U. Hwang, N. J. Lee, G. Jeong and Y.-J. Kim, *Chemical Communications*, 2012, **48**, 5455-5457.
8. X. Wu, H. Xu, L. Lu, H. Zhao, J. Fu, Y. Shen, P. Xu and Y. Dong, *Journal of Power Sources*, 2014, **250**, 274-278.
9. W. H. Wang and X. D. Wang, *Electrochimica Acta*, 2007, **52**, 6755-6762.
10. R.-H. Huang, C.-H. Sun, T.-m. Tseng, W.-k. Chao, K.-L. Hsueh and F.-S. Shieu, *Journal of The Electrochemical Society*, 2012, **159**, A1579-A1586.